

# Crystal and magnetic structure of $\text{Ca}_3\text{Ru}_2\text{O}_7$

Yoshiyuki Yoshida\*

Japan Society for the Promotion of Science, Chiyoda, Tokyo 102-8471, Japan and Nanoelectronics Research Institute,  
National Institute of Advanced Industrial and Technology (AIST), Tsukuba, 305-8568, Japan

Shin-Ichi Ikeda, Hirofumi Matsuhata, and Naoki Shirakawa

Nanoelectronics Research Institute, National Institute of Advanced Industrial and Technology (AIST), Tsukuba, 305-8568, Japan

C. H. Lee

Energy Technology Research Institute, National Institute of Advanced Industrial and Technology (AIST), Tsukuba, 305-8568, Japan

Susumu Katano

Advanced Science Research Center, Japan Atomic Energy Research Institute (JAERI), Tokai, Ibaraki 319-1195, Japan

(Received 5 November 2004; revised manuscript received 6 June 2005; published 9 August 2005)

The crystal structure of the double-layered  $\text{Ca}_3\text{Ru}_2\text{O}_7$  has been studied by convergent beam electron diffraction and powder neutron diffraction. The temperature dependence of the diffraction pattern reveals that all the lattice constants jump at the first-order metal-nonmetal transition at 48 K without a change of the space group symmetry of  $Bb2_1m$ . In the neutron diffraction experiment, an additional magnetic reflection emerges below the Néel temperature, 56 K. A possible model for this antiferromagnetic ordering is proposed, in which model magnetic moments align ferromagnetically within the double layer and antiferromagnetically between the double layers. This model reasonably explains the characteristic field dependence of the magnetoresistance observed at around 6 T.

DOI: [10.1103/PhysRevB.72.054412](https://doi.org/10.1103/PhysRevB.72.054412)

PACS number(s): 75.25.+z, 75.47.De, 61.12.Ex, 61.14.Lj

## I. INTRODUCTION

Ruddlesden-Popper (RP) type ruthenates  $(\text{Sr}, \text{Ca})_{n+1}\text{Ru}_n\text{O}_{3n+1}$  have attracted many researchers since the discovery of the spin-triplet superconductivity in  $\text{Sr}_2\text{RuO}_4$  ( $n=1$ ).<sup>1</sup> Beside the superconductivity, these ruthenates show a wide variety of magnetic and transport properties. For example, double-layered  $\text{Sr}_3\text{Ru}_2\text{O}_7$  ( $n=2$ ) shows the Fermi-liquid behavior, and ferromagnetic instability in the ground state, which has been lately discussed in terms of a quantum criticality tuned by magnetic field.<sup>2,3</sup> A recent report revealed that a ferromagnetic ordering emerged under uniaxial pressures above 0.1 GPa.<sup>4</sup> The crystal structure is a distorted RP type structure with an orthorhombic space group  $Bbcb$  (No. 68),<sup>5</sup> where  $\text{RuO}_6$  octahedra rotate around the  $c$  axis. Such a distortion may play an important role in magnetic properties of  $\text{Sr}_3\text{Ru}_2\text{O}_7$ . It is therefore interesting to investigate how a structural distortion relates to physical properties in RP type ruthenates.

$\text{Ca}_3\text{Ru}_2\text{O}_7$  has a more distorted crystal structure than  $\text{Sr}_3\text{Ru}_2\text{O}_7$  because the ionic radius of  $\text{Ca}^{2+}$  is rather smaller than that of  $\text{Sr}^{2+}$ . The crystal structure has the orthorhombic symmetry with  $Bb2_1m$  space group (No. 36) (or  $Cmc2_1$  with  $a$  being the long axis) with rotation and tilting of  $\text{RuO}_6$  octahedra, as shown in Fig. 1.<sup>6,7</sup>

The physical properties of single crystalline  $\text{Ca}_3\text{Ru}_2\text{O}_7$  have been reported for both flux grown and floating-zone (FZ) crystals. The first paper on flux-grown single crystals reported that  $\text{Ca}_3\text{Ru}_2\text{O}_7$  shows metallic antiferromagnetism (AFM) between the first-order metal-to-nonmetal transition temperature ( $T_{\text{MI}}=48$  K) and AFM ordering (Néel) tempera-

ture ( $T_{\text{N}}=56$  K).<sup>8</sup> It was also reported that  $\text{Ca}_3\text{Ru}_2\text{O}_7$  has substantial electronic specific heat coefficient  $\gamma = 22$  mJ/Ru mol  $\text{K}^2$  even in the insulating state, where the Shubnikov-de Haas oscillations with a very low frequency are observed.<sup>7,9,10</sup>

On the other hand, the report on FZ crystals revealed that  $\text{Ca}_3\text{Ru}_2\text{O}_7$  has a quasi-two-dimensional metallic ground state below 30 K, from which the quantum oscillations derive.<sup>11</sup>

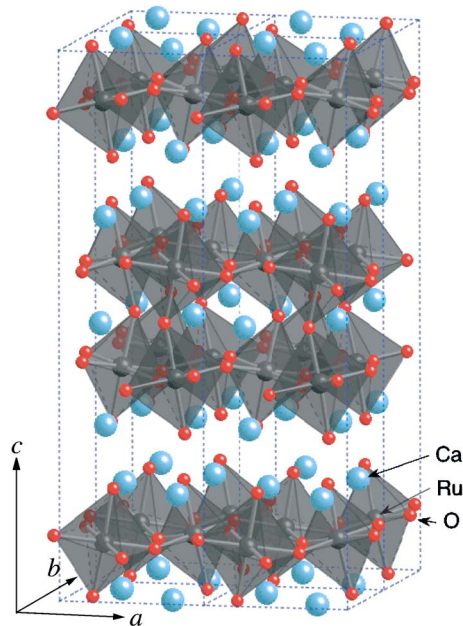


FIG. 1. (Color online) Crystal structure of  $\text{Ca}_3\text{Ru}_2\text{O}_7$ . Four unit cells are shown in this figure.

In this report,  $\gamma$  was estimated to be 1.7 mJ/Ru mol K<sup>2</sup>, which is ten times smaller than that of flux crystals. Such distinct differences of the physical properties between the flux and the FZ crystals are still open questions to be settled.

Recently, the jumps in the lattice constants were observed at the first-order transition temperature from x-ray diffraction and thermal contraction measurements.<sup>10,12</sup> However, it is not clear whether the space group symmetry of the crystal structure changes at the first-order transition. Concerning the magnetic structure in the AFM ordering, McCall *et al.* speculated from the magnetization measurements that the magnetic moments are ferromagnetically aligned within planes and coupled antiferromagnetically between the planes (A-type AF structure).<sup>7</sup> In defining the A-type AF structure in bilayered RP type oxides, we can either regard one bilayer as a single entity or as two individual adjacent layers. In the former case, the bilayer is a ferromagnetic entity stacked antiferromagnetically along the  $c$  axis. In the latter, the bilayer is made up of two antiferromagnetically coupled layers, either of which has a ferromagnetic spin structure. The magnetic structure needs to be directly confirmed with neutron diffraction measurements.

To clarify the temperature dependence of the structural parameters and the magnetic structure in the ground state, we carried out convergent beam electron diffraction (CBED) and powder neutron diffraction measurements. We have obtained the structural parameters at each temperature and propose the magnetic structure in the ground state of Ca<sub>3</sub>Ru<sub>2</sub>O<sub>7</sub>.

## II. EXPERIMENT

We grew single crystals of Ca<sub>3</sub>Ru<sub>2</sub>O<sub>7</sub> by a floating-zone (FZ) method with a commercial FZ furnace (Crystal System, Model FZ-T-10000-H-II-P-M). The crystal growth was performed in an atmosphere of the mixture of Ar and O<sub>2</sub> (Ar:O<sub>2</sub>=9:1). As-grown crystals were used for the measurements. Thin specimens of the single crystal for transmission electron microscopy (TEM) were prepared through ion milling. The powder sample for neutron diffraction was crushed from the single crystals.

TEM observations were carried out using a JEM 4000FX instrument operated at 100–200 kV at room temperature (RT) and 20 K. Parallel-beam-diffraction and CBED patterns were observed at various crystallographic orientations. A double-tilt He cooling stage was used for the measurement at 20 K. The leakage of magnetic field from the objective electron lens is in the range of 2 T at the specimen.

Neutron diffraction patterns were collected with a high resolution powder diffractometer (HRPD) installed at the JRR-3M reactor in JAERI, Tokai. This diffractometer uses 64 detectors, and the angles between the detectors are about 2.5°. The incident neutron wave length was 1.823 Å, and the collimation was set at 6'-20'-6'. The intensities were measured with the step of an angle of 0.05°. A vanadium sample cell with a diameter of 10 mm was used to avoid diffraction peaks from the cell. This sample cell was placed in an Al filled with He gas, then mounted in a conventional cryocooler. The diffraction patterns were obtained at the temperatures between RT and 8 K.

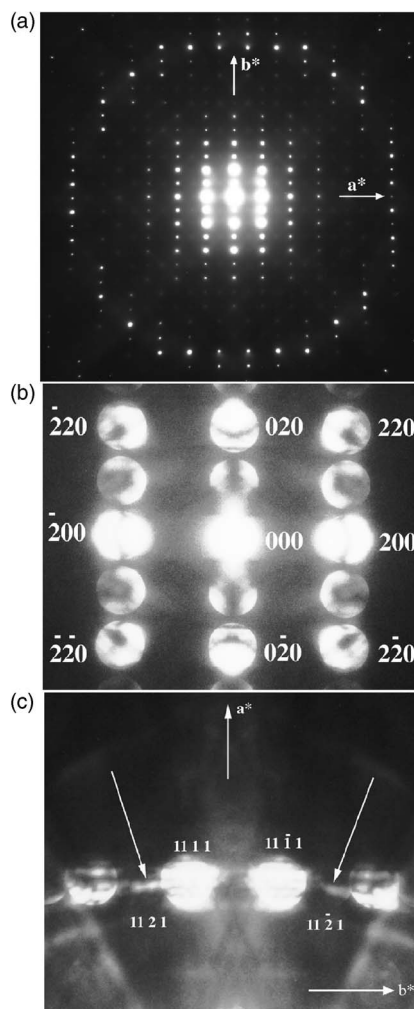


FIG. 2. (a) Parallel beam electron diffraction pattern and (b), (c) CBED patterns observed at the [001] zone axis at room temperature.

## III. RESULTS AND DISCUSSION

### A. Space group of Ca<sub>3</sub>Ru<sub>2</sub>O<sub>7</sub>

To clarify the precise space group symmetry, the observations of both parallel beam diffraction and CBED patterns were performed at RT and 20 K. Parallel-beam electron diffraction pattern and CBED patterns observed from the [001] zone axis at RT are shown in Figs. 2(a)–2(c). From CBED patterns, the Gjønnnes-Moodie lines are seen as a dark line in (0k0) disks ( $k=2n+1$ ), as shown in Fig. 2(b). These Gjønnnes-Moodie lines in the CBED pattern and the extinction rule in the parallel beam patterns suggest three candidates for the space group of Ca<sub>3</sub>Ru<sub>2</sub>O<sub>7</sub>, which are *Bbm*2 (No. 40), *Bbmm* (No. 63), and *Bb*2<sub>1</sub>*m* (No. 36). All three models are *B*-face centered cells and have glide symmetry along the  $b$  axis. In addition to this, the CBED pattern in Fig. 2(c) revealed that the mirror symmetry is broken perpendicular to the  $b^*$  axis. Taking into account the extinction rule and this fact, the space group of Ca<sub>3</sub>Ru<sub>2</sub>O<sub>7</sub> at RT is limited to *Bb*2<sub>1</sub>*m*, which is intrinsically the same as the previously reported one *A*2<sub>1</sub>*ma* (No. 36).<sup>6</sup> The difference of the expression between

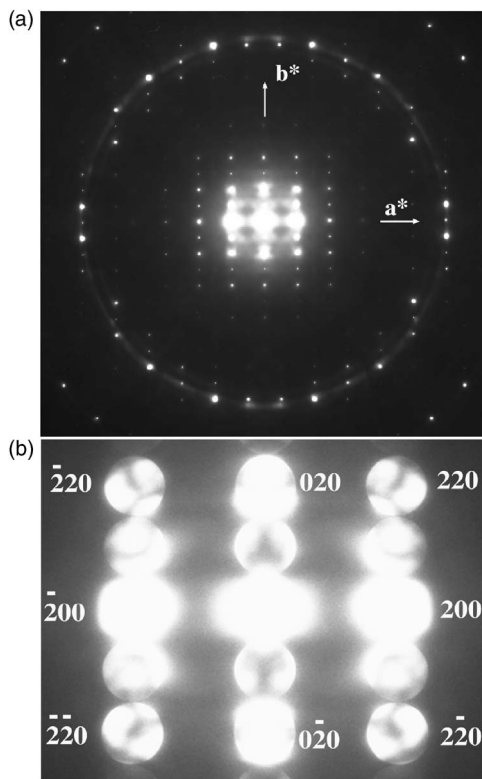


FIG. 3. (a) Parallel beam electron diffraction pattern and (b) CBED pattern observed at the  $[001]$  zone axis at 20 K.

$A2_1ma$  and  $Bb2_1m$  simply originates from the definition of the crystallographic axes.<sup>13</sup>

Figures 3(a) and 3(b) show a parallel beam electron diffraction pattern and CBED pattern observed at the  $[001]$  zone axis at 20 K, respectively. Neither an additional reflection nor a CBED pattern was observed at 20 K when compared with the result at RT, indicating that the space group of  $Bb2_1m$  is retained down to 20 K. This result shows that the space group symmetry of  $\text{Ca}_3\text{Ru}_2\text{O}_7$  is not affected by the structural distortion at 48 K. A similar behavior was also reported for the single-layered  $\text{Ca}_2\text{RuO}_4$ .<sup>14</sup>

### B. Crystal structure of $\text{Ca}_3\text{Ru}_2\text{O}_7$

Neutron diffraction patterns were obtained at various temperatures from RT to 8 K. The typical diffraction pattern at RT is shown in Fig. 4. Structure refinements were made for  $\text{Ca}_3\text{Ru}_2\text{O}_7$  at each temperature with a Rietveld refinement program RIETAN.<sup>15</sup> Some ranges in the scattering angle were excluded below the Néel temperature, due to the existence of the magnetic scattering. On the basis of the result of CBED, the space group of the crystal was fixed on  $Bb2_1m$ . In the diffraction pattern, some impurity peaks were observed. These peaks originate from  $\text{Ca}_2\text{RuO}_4$  and  $\text{CaRuO}_3$  phases. In the Rietveld analysis, a multiphase fitting was performed. As a result, the obtained  $R$  factors for each temperature are in the range from 7.56 to 9.86%. The amounts of impurity phases are determined to be 1 and 5 wt % for  $\text{Ca}_2\text{RuO}_4$  and  $\text{CaRuO}_3$ , respectively.

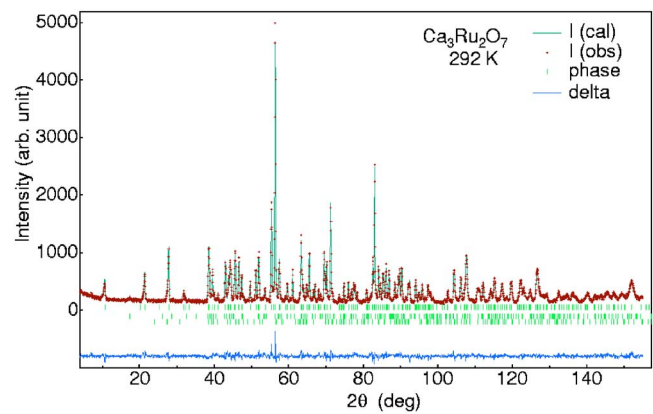


FIG. 4. (Color online) Neutron diffraction pattern obtained with HRPD for  $\text{Ca}_3\text{Ru}_2\text{O}_7$  together with the corresponding calculated profile. The upper row of the vertical bars shows the positions of the Bragg reflections from the main  $\text{Ca}_3\text{Ru}_2\text{O}_7$  phase. The lower two rows indicate those of the impurity  $\text{Ca}_2\text{RuO}_4$  and  $\text{CaRuO}_3$  phases, which were estimated to be 6 wt % in total.

The temperature dependences of the obtained structural parameters are listed together with  $R$ -factors in Table I. The final structural parameters at RT are consistent with those in the previous report.<sup>6</sup> The calculated profile and the positions of the Bragg reflections at RT are also shown in Fig. 4.

Figures 5(a)–5(c) show the temperature dependence of the lattice constants  $a$ ,  $b$ , and  $c$ , respectively. The lattice constants  $a$  and  $c$  shorten on cooling from RT, while  $b$  elongates. As shown in the previous reports,<sup>10,12</sup> the lattice parameters jump at the first-order transition temperature of 48 K. From the x-ray diffraction measurements on the flux-grown crystals, the lattice constant  $c$  changes at the transition while  $a$  and  $b$  do not change.<sup>10</sup> The thermal contraction measurement of a FZ crystal was performed only for the lattice constant  $a$ , which jumps at the transition.<sup>12</sup> The present experiment reveals that all the lattice constants change at the transition. Here  $c$  shortens by about 0.1%, while both  $a$  and  $b$  lengthen by about 0.07%. This result does not agree with the result from the x-ray diffraction on the crystal by the flux method.<sup>10</sup> The lattice volume increases at this transition, as shown in Fig. 5(d). The behavior around the structural transition of  $\text{Ca}_3\text{Ru}_2\text{O}_7$  is similar to that of  $\text{Ca}_2\text{RuO}_4$ .<sup>14</sup> However, there is a difference in the temperature dependence below the transition temperature. Below 48 K, the lattice constants of  $\text{Ca}_3\text{Ru}_2\text{O}_7$  are almost independent of temperature, but those of  $\text{Ca}_2\text{RuO}_4$  decrease with decreasing temperature. The structural transition temperature of this compound is much lower than that of  $\text{Ca}_2\text{RuO}_4$ , 357 K. This might be the reason that the lattice constants are almost constant below the transition temperature in  $\text{Ca}_3\text{Ru}_2\text{O}_7$ .

Figures 6(a) and 6(b) show temperature dependences of bond lengths in the  $\text{RuO}_6$  octahedra and bond angles in the octahedra in  $\text{Ca}_3\text{Ru}_2\text{O}_7$ , respectively. The error is denoted by the error bars in the figures. In Fig. 6(a), error bars are shown only for selected points to clarify the data points. Although the estimated error bars are rather large, the temperature dependences of the bond lengths show characteristic features above the transition temperature. The lengths of Ru–O(1) and Ru–O(3) bonds increase with decreasing temperature.

TABLE I. Results of the Rietveld analyses on  $\text{Ca}_3\text{Ru}_2\text{O}_7$  at various temperatures. Errors are in parentheses and result from the least-squares fitting. The origin along  $y$  parameters is defined as the middle point of the line connecting the two Ru atoms that are mapped to one another by a twofold screw rotation along the  $b$  axis at room temperature.

Temperature		292 K	120 K	60 K	50 K	40 K	30 K	20 K	8 K
Space group		$Bb2_1m$	$Bb2_1m$	$Bb2_1m$	$Bb2_1m$	$Bb2_1m$	$Bb2_1m$	$Bb2_1m$	$Bb2_1m$
$a$ (Å)		5.3781(2)	5.3648(2)	5.3632(2)	5.3637(2)	5.3676(2)	5.3677(2)	5.3678(2)	5.3677(2)
$b$ (Å)		5.5227(2)	5.5295(2)	5.5315(2)	5.5325(2)	5.5351(2)	5.5354(2)	5.5356(2)	5.5356(2)
$c$ (Å)		19.5872(8)	19.5493(7)	19.5405(7)	19.5375(7)	19.5221(7)	19.5221(7)	19.5209(7)	19.5212(9)
$V$ (Å <sup>3</sup> )		581.78(4)	579.94(3)	579.71(3)	579.78(3)	580.02(3)	580.06(3)	580.06(3)	580.05(4)
$R_{\text{wp}}$ (%)		7.94	7.56	7.68	7.72	8.03	7.91	7.96	9.86
$R_e$ (%)		5.98	5.01	5.01	5.01	5.01	5.01	4.99	7.73
$S$		1.33	1.51	1.53	1.54	1.60	1.58	1.59	1.27
Ru	$x$	0.2504(7)	0.2541(6)	0.2534(6)	0.2525(7)	0.2518(7)	0.2526(7)	0.2527(7)	0.2533(9)
$8b$	$y$	0.7500(13)	0.7503(12)	0.7502(11)	0.7500(12)	0.7508(12)	0.7502(12)	0.7505(11)	0.7512(14)
	$z$	0.4008(2)	0.4011(2)	0.4012(1)	0.4010(2)	0.4012(2)	0.4010(2)	0.4011(2)	0.4011(2)
$U_{\text{iso}}$		0.0063(6)	0.0065(6)	0.0053(6)	0.0056(6)	0.0063(7)	0.0066(7)	0.0072(7)	0.0060(8)
Ca(1)	$x$	0.7394(19)	0.7400(12)	0.7385(12)	0.7373(12)	0.7381(12)	0.7372(12)	0.7370(12)	0.7382(15)
$4a$	$y$	0.2011(19)	0.1973(17)	0.1967(17)	0.1960(17)	0.1961(18)	0.1947(18)	0.1947(18)	0.1949(22)
	$z$	0	0	0	0	0	0	0	0
$U_{\text{iso}}$		0.0068(16)	0.0076(15)	0.0053(15)	0.0051(15)	0.0064(15)	0.0069(15)	0.0071(15)	0.0042(19)
Ca(2)	$x$	0.2464(9)	0.2450(8)	0.2455(8)	0.2456(8)	0.2466(8)	0.2465(8)	0.2457(7)	0.2443(10)
$8b$	$y$	0.3005(18)	0.3026(15)	0.3034(15)	0.3030(16)	0.3052(17)	0.3037(17)	0.3043(8)	0.3036(20)
	$z$	0.3115(2)	0.3109(2)	0.3110(2)	0.3109(2)	0.3111(2)	0.3109(2)	0.3108(2)	0.3112(2)
$U_{\text{iso}}$		0.0125(13)	0.0073(13)	0.0067(12)	0.0065(12)	0.0076(12)	0.0075(12)	0.0072(12)	0.0063(15)
O(1)	$x$	0.8163(5)	0.8168(5)	0.8177(5)	0.8176(5)	0.8179(5)	0.8186(5)	0.8180(5)	0.8188(6)
$8b$	$y$	0.2334(14)	0.2325(8)	0.2318(8)	0.2320(8)	0.2330(9)	0.2322(9)	0.2316(13)	0.2309(12)
	$z$	0.6987(2)	0.6988(1)	0.698(1)	0.6986(2)	0.6986(2)	0.6987(1)	0.6987(2)	0.6987(2)
$U_{\text{iso}}$		0.0125(8)	0.0089(9)	0.0062(8)	0.0078(9)	0.0069(9)	0.0067(9)	0.0081(9)	0.0075(12)
O(2)	$x$	0.3341(9)	0.3375(8)	0.3378(8)	0.3377(8)	0.3383(9)	0.3381(9)	0.3375(8)	0.3370(10)
$4a$	$y$	0.7735(19)	0.7737(17)	0.7737(17)	0.7736(17)	0.7730(18)	0.7733(18)	0.7721(18)	0.7702(19)
	$z$	1/2	1/2	1/2	1/2	1/2	1/2	1/2	1/2
$U_{\text{iso}}$		0.0148(14)	0.0083(12)	0.0079(12)	0.0070(12)	0.0069(9)	0.0114(13)	0.0084(13)	0.0081(17)
O(3)	$x$	0.4478(7)	0.4479(6)	0.4484(6)	0.4477(6)	0.4480(6)	0.4478(6)	0.4471(6)	0.4474(7)
$8b$	$y$	0.9499(14)	0.9497(13)	0.9499(13)	0.9494(13)	0.9512(14)	0.9494(14)	0.9506(14)	0.9500(13)
	$z$	0.0823(2)	0.0817(2)	0.0818(2)	0.0817(2)	0.0816(2)	0.0815(2)	0.0815(2)	0.0819(2)
$U_{\text{iso}}$		0.0100(8)	0.0082(9)	0.0074(9)	0.0073(9)	0.0089(10)	0.0087(9)	0.0086(8)	0.0059(11)
O(4)	$x$	0.9505(7)	0.9472(5)	0.9473(5)	0.9475(5)	0.9483(6)	0.9479(5)	0.9486(6)	0.9481(7)
$8b$	$y$	0.0495(14)	0.0468(13)	0.0461(13)	0.0459(13)	0.0473(14)	0.0488(14)	0.0459(14)	0.0458(16)
	$z$	0.1162(2)	0.1159(2)	0.1161(2)	0.1161(2)	0.1160(2)	0.1161(2)	0.1161(2)	0.1162(2)
$U_{\text{iso}}$		0.0098(9)	0.0057(9)	0.0043(8)	0.0047(9)	0.0056(9)	0.0057(9)	0.0048(9)	0.0055(11)

On the other hand, those of Ru–O(2) and Ru–O(4) decrease with decreasing temperature. At the structural transition, a noticeable change of the bond length cannot be observed except for the distance of Ru–O(4). It lengthens by about 0.4% at the transition temperature. On the other hand, in the single-layered  $\text{Ca}_2\text{RuO}_4$ , the bond lengths jump at the structural transition and show larger temperature dependences below the transition than those of  $\text{Ca}_3\text{Ru}_2\text{O}_7$ .<sup>14</sup> In  $\text{Ca}_2\text{RuO}_4$ , the

in-plane Ru–O bonds become elongated by about 1%, while the out-of-plane ones shrink by about 1%, at the transition upon cooling.

With respect to the angles between the  $\text{RuO}_6$  octahedra, which are shown in Fig. 6(b), they are almost temperature independent above  $T_N$  and little affected by the structural transition. However, some characteristic temperature dependences can be observed below 40 K. The angle of



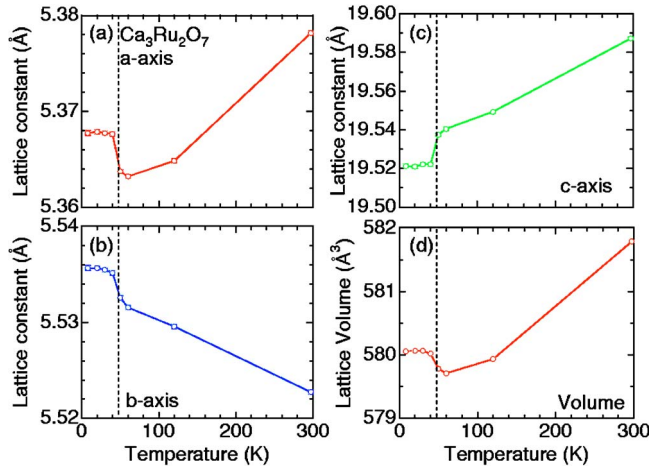


FIG. 5. (Color online) Temperature dependences of lattice constants (a)  $a$ , (b)  $b$ , (c)  $c$ , and (d) the lattice volume of  $\text{Ca}_3\text{Ru}_2\text{O}_7$ . Solid lines are connected between the data points. The broken lines denote the structural transition temperature of 48 K.

$\text{Ru}-\text{O}(1)-\text{Ca}(2)$  decreases with decreasing temperature. On the other hand, the angle of  $\text{Ru}-\text{O}(2)-\text{Ru}$  increases with decreasing temperature. Considering the crystal structure of  $\text{Ca}_3\text{Ru}_2\text{O}_7$ , which consists of the  $\text{RuO}_6$  double layer and  $\text{CaO}$  layer (see Fig. 7), these results imply that the electron transfer increases within the double layer and that the transfer decreases between the double layers below 30 K. This behavior of the bond angles might explain the quasi-two-dimensional transport properties of  $\text{Ca}_3\text{Ru}_2\text{O}_7$ .<sup>11</sup>

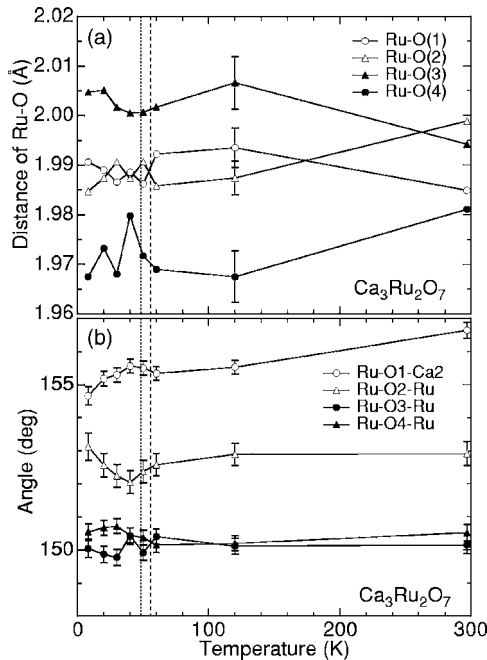


FIG. 6. Temperature dependences of (a) bond lengths of the  $\text{RuO}_6$  octahedra and (b) angles between the octahedra in  $\text{Ca}_3\text{Ru}_2\text{O}_7$ . Solid lines are connected between the data points. The broken and dotted lines denote the Néel temperature (56 K) and the structural transition temperature (48 K), respectively.

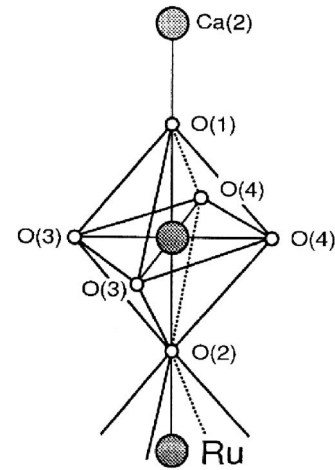


FIG. 7. Atomic sites around  $\text{RuO}_6$  octahedron in  $\text{Ca}_3\text{Ru}_2\text{O}_7$ .

### C. Magnetic structure of $\text{Ca}_3\text{Ru}_2\text{O}_7$

Figure 8 shows diffraction patterns of  $\text{Ca}_3\text{Ru}_2\text{O}_7$  in the low-angle range from  $4^\circ$  to  $18^\circ$  at various temperatures. On cooling below  $T_N$ , an additional reflection emerges, which is indexed with (001) on the assumption of the  $Bb2_1m$  lattice. This peak does not satisfy the extinction rule of the  $Bb2_1m$  symmetry, and corresponds to the magnetic scattering due to the antiferromagnetic ordering.<sup>16</sup> The (001) reflection is clearly observed in the diffraction pattern; however, the possible reflections at higher angles, such as (003) or (005), etc., are not observed clearly.

As to the magnetic structure of  $\text{Ca}_3\text{Ru}_2\text{O}_7$ , McCall *et al.* proposed a magnetic structure with the A-type antiferromagnetic ordering, which was speculated from the magnetization measurements.<sup>7</sup> Here, we analyze the magnetic structure directly from the neutron diffraction data. Taking account of the fact that the only observed reflection is the (001), we can exclude the magnetic structure with the  $Bb2_1m$  symmetry, and can assume ones with the propagation vector along the  $c$  axis. As a result, the possible magnetic structures can be limited to two models shown in Figs. 9(a) and 9(b). In these

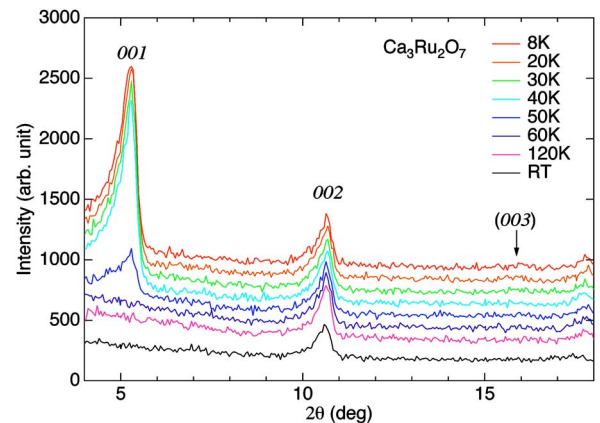
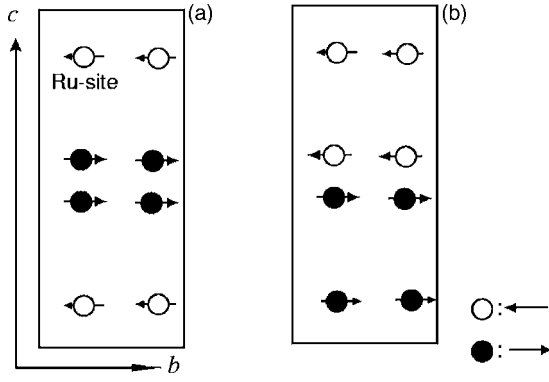


FIG. 8. (Color online) Diffraction patterns of  $\text{Ca}_3\text{Ru}_2\text{O}_7$  at low angles showing the (001) and (002) reflections at various temperatures.

FIG. 9. Two possible magnetic structures of  $\text{Ca}_3\text{Ru}_2\text{O}_7$ .

figures, the direction of the magnetic moments ( $\parallel b$ ) was assumed from the results of magnetization.<sup>7,11–13</sup>

To clarify which model is more suitable for the magnetic ground state, we calculated the magnetic intensity of the diffraction pattern for both models by the computing program. In this calculation, the following expression of the magnetic intensity is used:<sup>17,18</sup>

$$I \propto \sum_{\{h,k,l\}} j_{\{h,k,l\}} (1 - \langle \cos^2 \eta \rangle) |F(m)_{\{h,k,l\}}|^2 \times L.F. \quad (1)$$

Here,  $j_{\{h,k,l\}}$  is the multiplicity of the magnetic structure factor  $F(m)_{\{h,k,l\}}$ ,  $\eta$  in the  $\langle \cos^2 \eta \rangle$  is the angle between the scattering vector and the magnetic moment of the scattering atom, and  $L.F.$  is the Lorentz factor, which is  $1/(\sin \theta \sin 2\theta)$  in a powder case. The magnetic structure factor is expressed as

$$F(m)_{\{h,k,l\}} = \sum_i (\gamma e^2 / 2m_e c^2) \mu_{eff} f(Q) \times \exp[2\pi j(hx_i + ky_i + lz_i)], \quad (2)$$

where  $\gamma$  is the neutron magnetic moment in nuclear magnetons,  $\mu_{eff}$  is a total moment on each site, and  $f(Q)$  is the magnetic form factor. The magnetic form factor for each reflection was obtained according to the formula in Ref. 17. From the results of the calculation, the Lorentz factors for both models were 232.6 for (001), and 25.9 for (003). Consequently, the ratio of the magnetic intensity between (003) and (001),  $I_{(003)}/I_{(001)}$ , was estimated to be 0.013 and 0.235 for the model (a) and (b), respectively. It is therefore expected that the reflection at (003) cannot be observed in the model (a), while it should be clearly observed in the model (b). We conclude from these results that the model (a) can explain the experimental data.

The value of the magnetic moment of Ru was estimated through comparing magnetic and nuclear intensities, i.e., the intensity ratio between (001) and (002) in Fig. 8. The estimated magnetic moment  $\mu_{eff}$  is  $1.59 \pm 0.07 \mu_B$ , which is smaller than the full ( $S=1$ ) moment of  $2\mu_B$ . This value is close to the moment after the metamagnetic transition for the field along the  $b$  axis in the magnetization measurements.<sup>7,12</sup> We also tried to fit the magnetic structure with the Rietveld refinements. However, the fitting did not converge satisfac-

torily enough, probably because the magnetic intensity appears clearly only at the (001) reflection and the profile of the peak observed at such rather low angles is considerably distorted. Nevertheless, the observed profile at 8 K can be reproduced reasonably well by the simulation with the magnetic structure and the magnetic moment obtained here. This fact ensures that our model is essentially correct.

In powder neutron diffraction, the direction of the magnetic moment can be estimated only from the  $\langle \cos^2 \eta \rangle$  term in Eq. (1). There is a possibility that the magnetic moment is not aligned along the crystallographic axis. However, it is difficult to determine the tilting angle of the magnetic moment since only one reflection was observed. From these analyses, we propose the model (a) as the most probable model for the magnetic structure of  $\text{Ca}_3\text{Ru}_2\text{O}_7$ .

In the magnetic susceptibility measurements, the magnetic anisotropy changes at the first-order transition temperature 48 K.<sup>10,11</sup> However, hardly any information about the magnetic anisotropy change is obtained from this measurement. As mentioned above, it is difficult to discuss the magnetic anisotropy from the powder neutron diffraction measurements. In addition, the magnetic intensity is still weak around 50 K since it is close to the Néel temperature. To discuss the magnetic structure in detail, we need to perform further neutron-diffraction studies using single crystals.

From these results, the magnetic structure of  $\text{Ca}_3\text{Ru}_2\text{O}_7$  is clarified in the ground state, where the magnetic moments align ferromagnetically within the double layer, while antiferromagnetically between the double layers. The magnetic structure obtained from this study is completely different from that of single-layered  $\text{Ca}_2\text{RuO}_4$ . This fact implies that the interaction within the double layer plays an important role for the determination of the magnetic ground state. Taking account of this magnetic structure, the field dependence of the magnetoresistance around 6 T is readily explained with the tunneling magnetoresistance (TMR), which was proposed in the previous reports.<sup>9,11</sup> It is also explained that ferromagnetic instability is predominant in the paramagnetic region, indicated by the positive Weiss temperatures in the magnetic susceptibility.<sup>7,11</sup> Recently, a similar feature was reported in the same bilayer ruthenate  $\text{Sr}_3\text{Ru}_2\text{O}_7$ . The inelastic neutron scattering measurement of  $\text{Sr}_3\text{Ru}_2\text{O}_7$  revealed that two-dimensional incommensurate magnetic fluctuations emerge at low temperature and that the fluctuations become predominately ferromagnetic above 20 K.<sup>19</sup> The uniaxial pressure induces ferromagnetic ordering in  $\text{Sr}_3\text{Ru}_2\text{O}_7$  above 0.1 GPa.<sup>4</sup> In addition to this, the Mott insulating  $\text{Ca}_2\text{RuO}_4$  turns into a FM metal under pressure.<sup>20</sup> It can be expected that these ferromagnetic interactions observed in other ruthenates are related to the magnetic structure of this  $\text{Ca}_3\text{Ru}_2\text{O}_7$ . The pressure study of  $\text{Ca}_3\text{Ru}_2\text{O}_7$  may be important in understanding the relation between the magnetic properties and crystal structure in double-layered ruthenates.

#### IV. CONCLUSION

We have studied the crystal and magnetic structures of  $\text{Ca}_3\text{Ru}_2\text{O}_7$  by convergent-beam electron diffraction and powder neutron diffraction. The temperature dependence of the

diffraction patterns revealed that all the lattice constants of  $\text{Ca}_3\text{Ru}_2\text{O}_7$  jump at the first-order transition temperature 48 K, though the space group symmetry of  $Bb2_1m$  is not affected throughout the temperature range measured.

On cooling below  $T_N=56$  K, an additional reflection emerges in the neutron diffraction patterns, corresponding to an antiferromagnetic ordering. In the magnetic ground state, the magnetic moments align ferromagnetically within the double layer, while antiferromagnetically between the double layers. This magnetic structure can explain the positive

Weiss temperature obtained in the paramagnetic phase and the field dependence of the magnetoresistance of  $\text{Ca}_3\text{Ru}_2\text{O}_7$ .

#### ACKNOWLEDGMENTS

The authors thank Y. Uwatoko, T. Yanagisawa, S. Koikegami, and S. Hara for their help and comments. We also thank Y. Ishii and Y. Shimojoh at JAERI for their help in performing the neutron powder diffraction experiments. This study is supported by domestic research fellowship on Japan Society for the Promotion of Science.

---

\*Electronic address: yoshida.y@aist.go.jp

- <sup>1</sup>Y. Maeno, T. M. Rice, and M. Sigrist, *Phys. Today* **54**, 42 (2001).
- <sup>2</sup>S. I. Ikeda, Y. Maeno, S. Nakatsuji, M. Kosaka, and Y. Uwatoko, *Phys. Rev. B* **62**, R6089 (2000).
- <sup>3</sup>S. A. Grigera, R. S. Perry, A. J. Schofield, M. Chiao, S. R. Julian, G. G. Lonzarich, S. I. Ikeda, Y. Maeno, A. J. Millis, and A. P. Mackenzie, *Science* **294**, 329 (2001).
- <sup>4</sup>S. I. Ikeda, N. Shirakawa, T. Yanagisawa, Y. Yoshida, S. Koikegami, S. Koike, M. Kosaka, and Y. Uwatoko, *J. Phys. Soc. Jpn.* **73**, 1322 (2004).
- <sup>5</sup>H. Shaked, J. D. Jorgensen, O. Chmaissem, S. Ikeda, and Y. Maeno, *J. Solid State Chem.* **154**, 361 (2000).
- <sup>6</sup>G. Cao, K. Abboud, S. McCall, J. E. Crow, and R. P. Guertin, *Phys. Rev. B* **62**, 998 (2000).
- <sup>7</sup>S. McCall, G. Cao, and J. E. Crow, *Phys. Rev. B* **67**, 094427 (2003).
- <sup>8</sup>G. Cao, S. McCall, J. E. Crow, and R. P. Guertin, *Phys. Rev. Lett.* **78**, 1751 (1997).
- <sup>9</sup>G. Cao, L. Balicas, Y. Xin, E. Dagotto, J. E. Crow, C. S. Nelson, and D. F. Agterberg, *Phys. Rev. B* **67**, 060406(R) (2003).
- <sup>10</sup>G. Cao, L. Balicas, Y. Xin, J. E. Crow, and C. S. Nelson, *Phys. Rev. B* **67**, 184405 (2003).
- <sup>11</sup>Y. Yoshida, I. Nagai, S. I. Ikeda, N. Shirakawa, M. Kosaka, and N. Mori, *Phys. Rev. B* **69**, 220411(R) (2004).
- <sup>12</sup>E. Ohmichi, Y. Yoshida, S. I. Ikeda, N. Shirakawa, and T. Osada, *Phys. Rev. B* **70**, 104414 (2004).
- <sup>13</sup>The space group No. 36 is represented by  $Cmc2_1$  in Ref. 16. In its alternative expression  $Bb2_1m$ , the lattice constants are arranged in order of the length with  $a < b < c$ . We have carefully checked crystal structure in this work, Refs. 11 and 12. These results clearly show that the “ $b$ ” axis is the magnetic easy axis in this  $Bb2_1m$  space group.
- <sup>14</sup>O. Friedt, M. Braden, G. Andre, P. Adelman, S. Nakatsuji, and Y. Maeno, *Phys. Rev. B* **63**, 174432 (2001).
- <sup>15</sup>F. Izumi and T. Ikeda, *Mater. Sci. Forum* **321–324**, 198 (2000).
- <sup>16</sup>*International Tables for Crystallography, Vol. A*, edited by T. Hahn (Kluwer Academic, Dordrecht, 2002).
- <sup>17</sup>G. Shirane, *Acta Crystallogr.* **12**, 282 (1959).
- <sup>18</sup>*International Tables for Crystallography, Vol. C*, edited by E. Prince (Kluwer Academic, Dordrecht, 2004).
- <sup>19</sup>L. Capogna, E. M. Forgan, S. M. Hayden, A. Wildes, J. A. Duffy, A. P. Mackenzie, R. S. Perry, S. Ikeda, Y. Maeno, and S. P. Brown, *Phys. Rev. B* **67**, 012504 (2003).
- <sup>20</sup>F. Nakamura, T. Goko, M. Ito, T. Fujita, S. Nakatsuji, H. Fukazawa, Y. Maeno, P. Alireza, D. Forsythe, and S. R. Julian, *Phys. Rev. B* **65**, 220402(R) (2002).